University of Reading

Effect of ENSO phase on large-scale snow water equivalent distribution in a GCM

Article

Published Version

Clifford, D., Gurney, R. J. and Haines, K. ORCID: https://orcid.org/0000-0003-2768-2374 (2009) Effect of ENSO phase on large-scale snow water equivalent distribution in a GCM. Journal of Climate, 22 (23). pp. 6153-6167. ISSN 1520-0442 doi: 10.1175/2009JCLI2993.1 Available at https://centaur.reading.ac.uk/1749/

It is advisable to refer to the publisher's version if you intend to cite from the work. See Guidance on citing.

To link to this article DOI: http://dx.doi.org/10.1175/2009JCLI2993.1

Publisher: American Meteorological Society

Publisher statement: © Copyright 2009 of the American Meteorological Society. The AMS Copyright Policy is available on the AMS web site at http://www.ametsoc.org.

All outputs in CentAUR are protected by Intellectual Property Rights law, including copyright law. Copyright and IPR is retained by the creators or other copyright holders. Terms and conditions for use of this material are defined in the End User Agreement.

University of Reading

www.reading.ac.uk/centaur

CentAUR

Central Archive at the University of Reading

Reading's research outputs online

Effect of ENSO Phase on Large-Scale Snow Water Equivalent Distribution in a GCM

DEBBIE CLIFFORD, ROBERT GURNEY, AND KEITH HAINES

National Centre for Earth Observation, Reading, United Kingdom

(Manuscript received 18 December 2008, in final form 25 June 2009)

ABSTRACT

Understanding links between the El Niño–Southern Oscillation (ENSO) and snow would be useful for seasonal forecasting, as well as for understanding natural variability and interpreting climate change predictions. Here, a 545-yr run of the third climate configuration of the Met Office Unified Model (HadCM3), with prescribed external forcings and fixed greenhouse gas concentrations, is used to explore the impact of ENSO on snow water equivalent (SWE) anomalies. In North America, positive ENSO events reduce the mean SWE and skew the distribution toward lower values, and vice versa during negative ENSO events. This is associated with a dipole SWE anomaly structure, with anomalies of opposite sign centered in western Canada and the central United States. In Eurasia, warm episodes lead to a more positively skewed distribution and the mean SWE is raised. Again, the opposite effect is seen during cold episodes. In Eurasia the largest anomalies are concentrated in the Himalayas. These correlations with February SWE distribution are seen to exist from the previous June–July–August (JJA) ENSO index onward, and are weakly detected in 50-yr subsections of the control run, but only a shifted North American response can be detected in the analysis of the 40-yr ECMWF Re-Analysis (ERA-40). The ENSO signal in SWE from the long run could still contribute to regional predictions, although it would only be a weak indicator.

1. Introduction

Forecasts of possible changes in land surface conditions are important both economically and politically, especially when examining impacts from climate change scenarios. It has been demonstrated that at midlatitudes, it is the land surface that dominates the uncertainty in general circulation model (GCM) responses (Crossley et al. 2000). However, the land surface has been given little attention in the context of GCMs, and observations are generally sparse. These issues were noted in the Intergovernmental Panel on Climate Change (IPCC) Fourth Assessment Report (AR4; Covey et al. 2003).

Snow plays a key role in the energy balance at the land–atmosphere boundary. Knowledge of the state of the snowpack over winter is also vital in forecasting water resources and wildfire risk in many parts of the world. Snow distribution is controlled by both temperature and precipitation fields, and as such makes a challenging diagnostic for climate models (Foster et al. 1996). As an accumulated property, it also provides an integrated measurement of recent seasonal variability. Seasonal predictions of snow anomalies might be possible by exploiting knowledge of the slower-varying components of the climate system, such as the ocean. The best-documented link between ocean variability and weather is the El Niño–Southern Oscillation (ENSO).

ENSO events have impacts on weather patterns across the globe, which may extend far enough to modulate the characteristics of Northern Hemisphere snow distribution. The IPCC AR4 describes how the representation of ENSO within the AR4 GCMs has improved in recent years and despite remaining biases, many of these models have been used for ENSO prediction, in particular the third climate configuration of the Met Office Unified Model (HadCM3) GCM (Covey et al. 2003).

Many studies relating snow to climate indices such as ENSO have been performed from an atmospheric dynamics perspective: exploiting snow information in order to predict the behavior of the atmosphere some weeks ahead (Leathers and Robinson 1993; Cohen and Entekhabi 1999; Cohen et al. 2007; Gong et al. 2007). These feedback processes, while important in representing climate and impacts in models properly, are not

Corresponding author address: Debbie Clifford, National Centre for Earth Observation, Department of Meteorology, University of Reading, Earley Gate, P.O. Box 243, Reading RG6 6BB, United Kingdom.
E-mail: d.j.clifford@reading.ac.uk

DOI: 10.1175/2009JCLI2993.1

© 2009 American Meteorological Society

the subject of this study. Here, the objective is reversed: can knowledge of ENSO phase be used to predict the state of the snowpack later in the season, or the following season? This would represent an important advance in improving the lead times for both hydrological and climate applications.

Work presented here shows the effect of ENSO phase on large-scale snow distribution [in this case snow water equivalent (SWE)] in a multicentury run of the HadCM3 general circulation model. By not confining studies to a small geographic area, and instead considering the whole Northern Hemisphere, the approach also tests the strength of remote connections in the model. By using a long model run, the robustness of the statistical relationship is not limited by a small number of ENSO events. While the mechanisms involved in these remote connections are important for both forecast interpretation and model diagnosis, a full investigation of these mechanisms is outside the scope of this paper. Here we are concerned with the response of a GCM to an ENSO event, as measured using SWE. This represents the first step in identifying relationships that could be exploited for forecasting in the future.

2. Previous work and background

Several studies have examined snow variability in the context of ENSO activity, but these have been concentrated on the North American continent. Jin et al. (2006) showed that 18% of the variability in measured SWE data in the western United States is ENSO driven, mainly due to changes in precipitation rather than temperature patterns. Clark et al. (2001) used station data to examine the influence of ENSO events on snowpack evolution in two North American river basins. Composites of mean anomalous snow in warm and cold phases are compared, and then used to predict runoff. This approach showed that, with the inclusion of ENSO information, there was skill in predicting spring runoff even before the snow begins to accumulate in the autumn. Sobolowski and Frei (2007) detected strong negative correlations between SWE in the Great Lakes region and October–November–December (OND) ENSO phase in the North American SWE reanalysis data of Brown et al. (2003). Shaman and Tziperman (2005) find correlations between January–February–March (JFM) Pacific SSTs and coincident spring and summer snow depth anomalies from satellite data on the Tibetan Plateau (although there are concerns about the behavior of the satellite snow depth retrieval over this region; Armstrong et al. 2004).

Further studies have investigated ENSO impacts on precipitation. Ropelewski and Bell (2008) examined the shift in the statistics of daily rainfall at stations in South America, with the ENSO phase. They find that useful information about the character of the rainfall season can be extracted, and they repeat the analysis using the station data in gridded form, and finally with rainfall statistics from the National Centers for Environmental Prediction–National Center for Atmospheric Research (NCEP–NCAR) reanalysis product. The gridded data reproduces many results from the station data, but not all the connections are seen when using reanalysis data. The authors attribute this discrepancy to biases in the reanalysis product. Ye (2001) shows a link between ENSO activity and Eurasian winter precipitation. Ye uses a principal components approach to detect teleconnections between variations in SSTs in the eastern Pacific and precipitation in southern-central Siberia.

Global precipitation was analyzed by Dai et al. (1997) using gridded station data for the years 1900–88. The first EOF of the dataset is a pattern related to ENSO, centered over the tropics, and ENSO is also shown to be the single largest cause of global extreme precipitation events. The authors also find trends in the global data (which are consistent with model-derived responses to increasing CO_2 levels) together with an increase in the elapsed time between dry events over the United States. The trends in the observed data, together with the difficulty of making accurate precipitation measurements with good spatial coverage, makes the patterns and mechanisms of interannual variability difficult to discern.

Although a climate model will always be an incomplete representation of reality, a GCM becomes an important tool for generating very long datasets that can be used for investigating mechanisms of variability. Understanding the interannual and decadal variability of climate models is essential in assessing the impact of external forcing on climate, and detecting and attributing trends (Collins et al. 2001). Observations will naturally contain the effects of both this internal variability and any externally driven trend; estimation of the effect of internal variability alone can only be performed within the controlled environment of a model. Investigation of connections within the internal variability of the model should also be a good test of the model, particularly for SWE distribution which is the result of subtle interactions between different atmospheric fields.

Observations of SWE at continental to hemispheric scales are only obtainable through remote sensing, and there remain many concerns about the reliability of the retrieval method (Andreadis and Lettenmaier 2006; Derksen 2008; Putt 2008). Passive microwave data was used by Yang et al. (1999) in a study of NCAR's Coupled Climate Model, version 3 (CCM3), and the authors

concluded that the GCM distribution was more reliable. For verification Yang et al. used a global snow dataset from the U.S. Air Force Environmental Technical Applications Center (Foster and Davy 1988), which used synoptic stations, literature searches, and climatological records to manually reconstruct a gridded hemispheric snow depth product. While this constitutes an independent, observation-based data source, Foster and Davy themselves acknowledge low confidence in data at high latitudes, and systematic biases have been identified by Brown and Frei (2007), which are particularly problematic over Eurasia. For this study of the whole Northern Hemisphere, a reanalysis product is used to provide an observational check on model results. While land surface data from reanalysis are generally considered less reliable than atmospheric data, there is no alternative source of global snow data with a long enough time series to cover a reasonable number of ENSO events. In this paper it is the result of atmospheric activity on snow distribution that is being tested, and while the land surface reanalysis in particular may have deficiencies, it is hoped that the atmospheric component would be driving anomalies of temperature and precipitation and hence the SWE anomalies.

Section 3 details the GCM and reanalysis products to be used, and outlines the method of detecting connections between SWE distribution and ENSO. Results are presented in section 4, and further discussion and conclusions are in sections 5 and 6.

3. Data and methodology

a. GCM: HadCM3

The model used in this study is the general circulation model HadCM3 from the Hadley Centre (Gordon et al. 2000), chosen because of its good ENSO representation. It is a fully coupled atmosphere–ocean model, which does not require flux adjustments. The land surface physics are described in Cox et al. (1999). The atmospheric component of HadCM3 has a resolution of 3.75° longitude by 2.5° latitude, and 19 vertical levels. The ocean component has a horizontal resolution of 1.25° by 1.25° with 20 vertical levels. While this resolution is relatively low, it is large-scale patterns that are to be investigated rather than local detail.

The representation of ENSO in HadCM3 is discussed in Slingo et al. (2003) and Guilyardi (2006). The latter showed that HadCM3 has an ENSO amplitude within ±20% of observations, and a good Pacific SST climatology. The response of the Indian Ocean to an ENSO event is well modeled, but an exaggerated response exists in the tropical Atlantic. The dominant ENSO frequency is also broadly correct, though there is some evidence that the model does not generate enough of a lower-frequency response (Guilyardi et al. 2004). HadCM3 is also capable of generating both modes that give rise to ENSO events as seen in observations (local SST–winds interactions in the central-east Pacific, and remote winds–thermocline feedbacks; Guilyardi 2006).

The SWE climatology of HadCM3 is consistent with that of the other GCMs that took part in the third round of the Coupled Model Intercomparison Project (CMIP; Brown and Mote 2009). The authors note the difficulty in validating large-scale SWE patterns because of a lack of a reliable global SWE climatology, and choose as their reference dataset the daily snow depth analyses produced by the Canadian Meteorological Center (Brasnett 1999) over the period 2001–06, converting to SWE using a density climatology. Compared to this hemispheric product, the CMIP GCMs (all of which had similar snow climatologies) showed somewhat higher SWE values at mid- to high latitudes, and higher SWE in the Himalayas. For the CMIP GCMs, such as HadCM3, the surface temperature was shown to be modeled with some confidence, while precipitation fields were less reliable (Covey et al. 2003).

To examine the internal variability of HadCM3, a multicentury ''control run'' has been studied. This 545-yr run includes solar and prescribed volcanic forcings, but fixed greenhouse gas forcings. This run was completed on a computing cluster, and was initialized from a spunup state from a much longer control run, to ensure the model components had reached equilibrium and there was no climatology drift.

The ENSO index used in this study is the seasonal SST anomaly in the Niño-3.4 box (5°N–5°S, 170°–120°W; Trenberth 1997), with an anomaly of greater than 0.5°C denoting a positive ENSO index, and less than −0.5°C being negative. While Trenberth proposes an ENSO definition based on a 0.4°C anomaly threshold, the standard deviation of SSTs in the Niño-3.4 box in this control run is somewhat higher than the observations quoted in the Trenberth paper (1.05° as opposed to 0.77°C) and the higher threshold of 0.5°C produces roughly the same proportion of positive and negative events over the 545-yr period as in the observations.

b. Reanalysis: ERA-40

The reanalysis product used to provide observational data is the 40-yr European Centre for Medium-Range Weather Forecasts (ECMWF) Re-Analysis (ERA-40). This is a widely used second-generation reanalysis product from ECMWF (Uppala et al. 2005). ERA-40 provides global climatologies of a range of surface and atmospheric variables for 44 yr over the time period from mid-1957 to mid-2002.

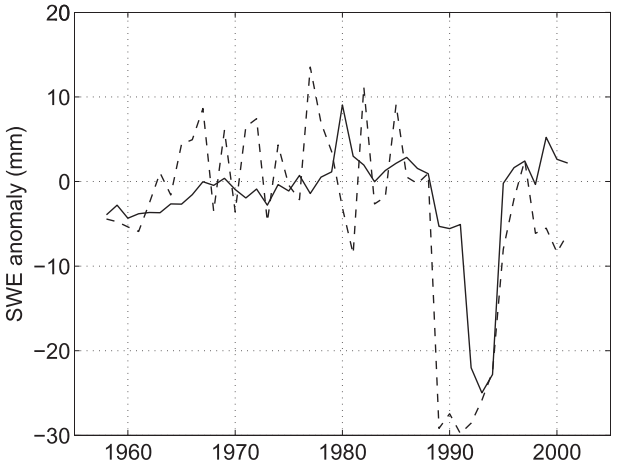

FIG. 1. Mean SWE anomaly time series (mm) from ERA-40 for North America (dashed) and Eurasia (solid). Anomalies are referenced to a 1958–87 ERA-40 SWE climatology.

The land surface scheme designed for the ERA-40 project is described in van den Hurk et al. (2000) and uses an explicit snowpack layer with prognostic equations for the snow albedo and density. The scheme also assimilates observed snow data from many stations worldwide, with the greatest coverage over North America. Evaluation of the land surface scheme in snow conditions showed that the new scheme improved snow depth, snowmelt timing, and turbulent fluxes above boreal forests, with beneficial impacts on the surface Bowen ratio and the atmospheric boundary layer.

Uppala et al. (2005) note that there is an error in the ERA-40 snow analysis between 1992 and 1994. Figure 1 shows the time series of anomaly SWE values in North America and Eurasia (referenced to the 1958–87 monthly climatology), which suggests that this error is actually present from 1989 onward, so all ERA-40 SWE data between 1989 and 1994 are omitted, leaving 38 yr of data for analysis.

c. Method

Composite February SWE anomalies are created to test whether there are lagged relationships between ENSO index and SWE distribution. February monthly averages have been chosen to be representative of the peak of the snow season, but before any melt occurs.

Four separate February SWE composites are created, based on the phase of the ENSO in the four seasons leading up to, and coincident with, the February SWE anomaly, specifically whether ENSO was positive in the March–April–May (MAM), June–July–August (JJA), September–October–November (SON), or December–January–February (DJF) prior to February. As an ENSO event will last for consecutive seasons, any given February SWE anomaly can occur in several groups. Similarly, composites are formed for negative phases of ENSO. The analysis was also performed with DJF and DJFM composites of monthly anomalies and results were qualitatively the same.

The precipitation study of Ropelewski and Bell (2008) used the Kolmogorov–Smirnov (K–S) test to determine whether the frequency distributions of precipitation data in positive and negative phases of ENSO were significantly different, and this approach is repeated here. The K–S test uses the maximum separation distance between the two cumulative frequency curves to determine whether the two distributions are statistically different (Smirnov 1948). The test is simple and nonparametric, though it will be applied to the anomaly difference between positive and negative ENSO phases for each grid box independently, so if positive and negative ENSO events have an impact in different regions, then an individual grid box may be less likely to pass the K–S test for significance.

The aim is to show whether the distribution of snow in February can be predicted from the ENSO phase in the preceding seasons. The approach is first applied to HadCM3, where the length of the control run allows the statistics to be robust. The ERA-40 reanalysis dataset however is less than 40 yr long, so to ascertain whether any connections found between SWE and ENSO phase should be detectable in the reanalysis data, the K–S test is also used on 5 consecutive 100-yr sections and ten 50-yr sections of the GCM control run to see whether the same connections are detected in the GCM over these shorter periods.

4. Analysis

a. HadCM3: 545-yr control run

Table 1 shows the effect of ENSO episodes on the frequency distribution of continental mean February SWE during the control run. The mean, standard deviation, and skewness for each of the distributions are listed. Significant differences between the distributions following positive and negative events are highlighted in bold (significance assessed using the K–S test with a threshold of 95%). The frequency distributions themselves for the DJF case are plotted in Fig. 2.

The February anomalies over North America that occur when ENSO is positive in DJF have the lowest mean, a high standard deviation, and the most positive skew, while those that occur when ENSO is negative in DJF have the highest mean, lowest standard deviation, and a negative skew (though a very low value at −0.07). Hence, the generally warmer climate in ENSO positive phases is leading to less snow over North America, but

TABLE 1. Statistics of continental mean February SWE with ENSO index in preceding MAM, JJA, SON, and coincident DJF. Seasons with statistically significant differences between positive and negative ENSO phases are in bold. Significance was assessed using a *t* test with a threshold of 95%.

			No. of years	Mean (mm)	Std dev (mm)	Skewness
North America	Whole run		545	83.4	5.15	0.16
	MAM	Positive	143	84.0	5.03	0.02
		Negative	152	82.8	5.52	0.27
	JJA	Positive	128	83.9	4.94	0.50
		Negative	132	83.3	5.54	0.32
	SON	Positive	**155**	**83.5**	**4.97**	**0.41**
		Negative	**164**	**83.5**	**5.37**	**0.10**
	DJF	Positive	**154**	**81.9**	**5.45**	**0.54**
		Negative	**179**	**84.9**	**4.90**	**−0.07**
Eurasia	Whole run		545	57.7	2.62	0.08
	MAM	Positive	143	57.1	2.36	0.34
		Negative	152	57.7	2.84	−0.13
	JJA	Positive	**128**	**57.3**	**2.51**	**0.18**
		Negative	**132**	**57.7**	**2.58**	**−0.29**
	SON	Positive	**155**	**57.1**	**2.70**	**0.30**
		Negative	**164**	**57.6**	**2.61**	**−0.28**
	DJF	Positive	**154**	**58.2**	**2.39**	**0.16**
		Negative	**179**	**56.7**	**2.75**	**0.06**

the high standard deviation and long positive tail of the distribution (as shown by the positive skew, and in Fig. 2) show that there are not consistently low snow values in every positive ENSO event: there are still many ENSO positive years with positive snow anomalies. A similar pattern is true for ENSO negative years, so while the climate is cooler and snow anomalies are generally positive, the negative skew means there are still low snow years among them.

For Eurasia, the statistics are mainly the opposite to the North American case: the positive ENSO phase in DJF brings a higher mean SWE and lower standard deviation, and vice versa for the negative phase. The changes in skewness however are similar to North America: the positive phase displays a more positive skew, while the negative phase shows a negative skew. It is interesting to note this difference between the continents: the warmer climate of ENSO positive events leads to deeper snow in Eurasia. The analysis was also performed with DJF and DJFM composites of monthly anomalies and results were qualitatively the same, but less significance was seen. It also appears that the response of Eurasian snow to ENSO may be more predictable than for North America, because the skewness is in the same direction as the change in mean values: for example, with both a higher mean and more positive skew in ENSO positive years, it is likely that a year with positive ENSO index also has a positive SWE anomaly.

Figure 3 shows the February SWE anomaly composites according to the ENSO index of a particular season (preceding MAM, JJA, SON, and coincident DJF, respectively). Examining first the SWE anomalies when the coincident DJF is positive (Fig. 3d), large positive anomalies are seen over the Himalayas. In North America a dipole pattern is seen, with large negative anomalies along the west coast and positive anomalies in the southern-central United States. This pattern is reproduced when considering DJF anomalies following a positive ENSO phase in SON and JJA (Figs. 3b,c, respectively), but not for positive ENSO phase in MAM (Fig. 3a).

Figure 4 shows the anomaly composites for February SWE following negative ENSO phases. The spatial pattern is very similar to that for the positive ENSO phase in Fig. 3, but with the sign of the anomalies reversed. Large negative anomalies occur over the Himalayas, and there are also negative anomalies farther east in China. The dipole pattern is seen once more in North America, with opposite-signed anomalies on the west coast and central United States. The same pattern is seen whether considering ENSO phase in the coincident DJF or preceding JJA and SON (Figs. 4b–d). In this case, the pattern is still seen when ENSO was negative in the preceding MAM (Fig. 4a).

To determine the significant differences in these anomaly patterns, the cumulative frequency distribution of SWE at each grid box is calculated for both positive and negative ENSO phases. These gridbox distributions are compared using the K–S test, again using a significance threshold of 95%. Figure 5 shows the K–S plot for February SWE anomalies, composited by ENSO phase in the preceding seasons (MAM, JJA,

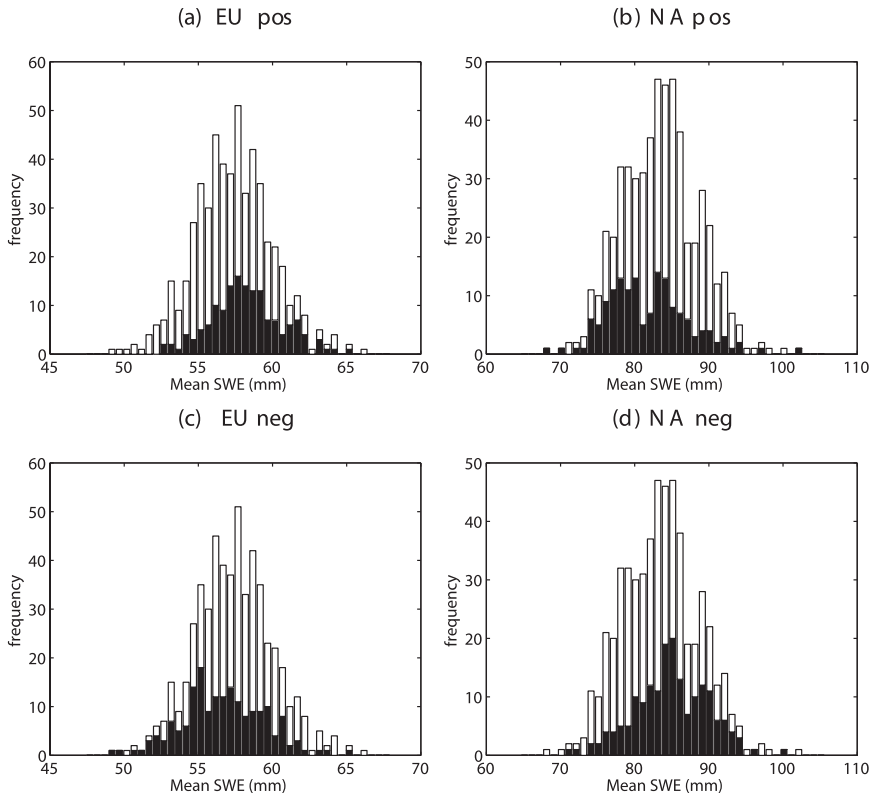

FIG. 2. Frequency distributions (in black) of continental mean SWE for (left) Eurasia and (right) North America when ENSO is (top) positive or (bottom) negative in DJF. White bars show the frequency distribution of mean February SWE from all years.

SON, and coincident DJF). The grid boxes, which have significantly different frequency distributions during opposite ENSO phases, are shaded. Figure 5d shows results for February anomalies that occur during DJF ENSO events. In North America, significant differences are found along the west coast and the southern United States, corresponding to the dipole pattern described earlier. In Eurasia, differences are seen across the Himalayas, China, and Japan.

Figure 5c for SON and Fig. 5b for JJA, both show patterns very similar to DJF in Fig. 5d, with some additional significance seen in Europe. Significance is much less widespread following MAM ENSO events (Fig. 5a).

The main Eurasian areas that are highlighted in Fig. 5, such as the Himalayas and parts of China, are areas of low latitude but high elevation, which could see increased snow even in a warmer ENSO positive climate if this were driving anomalously large precipitation. The shaded areas of significance generally correspond to regions that are known to be influenced by ENSO, such as western North America (Ropelewski and Halpert 1987), but also have large amounts of seasonal snow.

These results suggest that if a developing ENSO event can be detected or predicted in JJA or SON, the characteristics of the snowpack in the model the following February can also be forecast, providing a lead time of several months. But are these links only apparent in a very long model run, and, if real, could they be detected in the much shorter observational datasets available?

b. HadCM3: Shorter periods

Results for the K–S tests for consecutive 100-yr sections of the control run are shown in Fig. 6. The scale shows the number of 100-yr sections (0–5) in which that grid box displayed significant differences in SWE distribution in positive and negative ENSO phases. In the coincident DJF (Fig. 6d), significance is seen in the Himalayas, China, the west coast of North America, and the southern United States. Several of the grid boxes in the Himalayas and China are significant in at least four 100-yr sections.

In SON (Fig. 6c), significance is more limited across North America but grid boxes in the Himalayas and China still show significance. Figure 6b for JJA shows that significance in North America is now limited to the

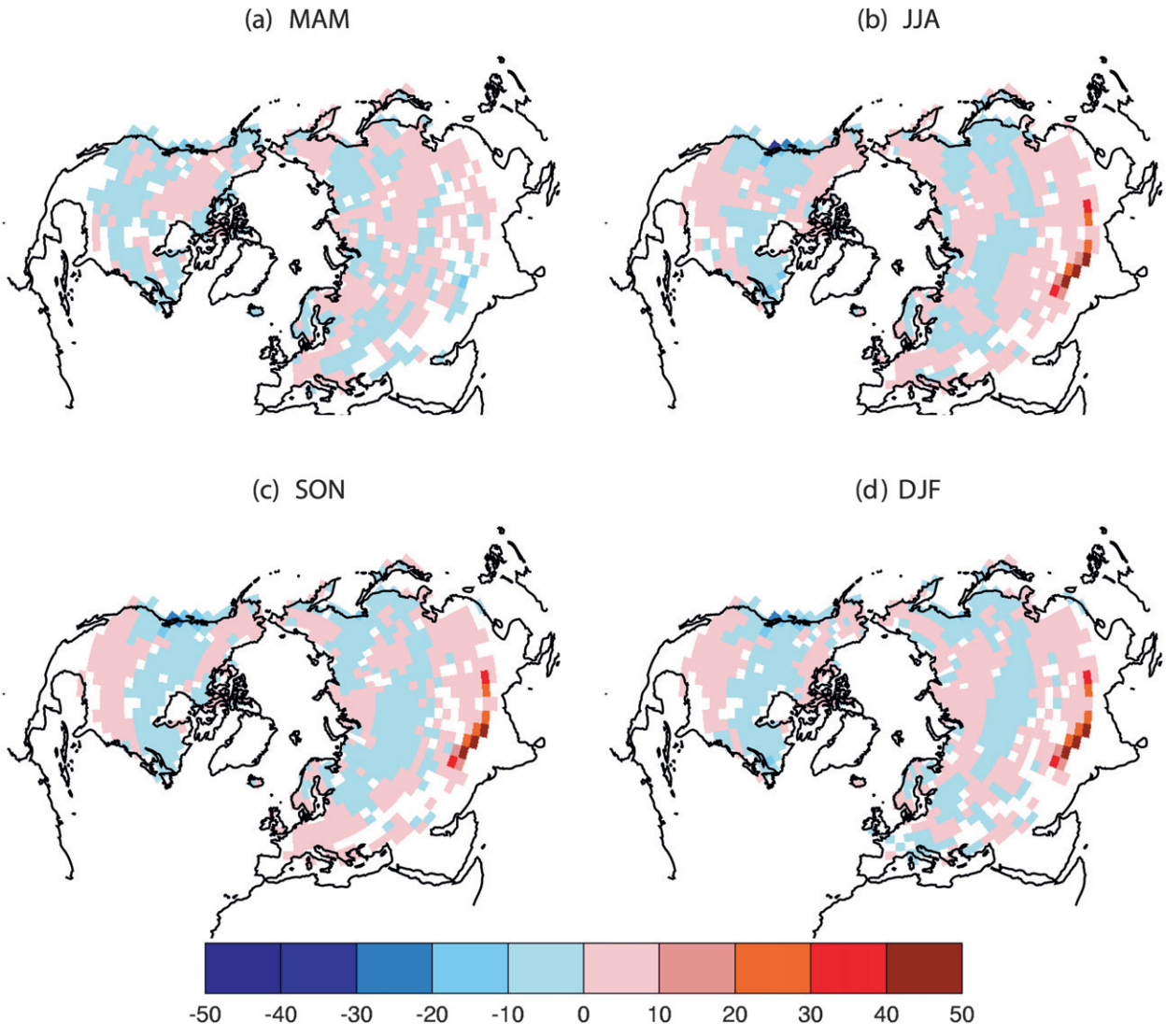

FIG. 3. February SWE anomaly distribution (mm) from years with positive ENSO index in the previous (a) MAM, (b) JJA, (c) SON, and (d) coincident DJF.

west coast, and in Eurasia to the Himalayas. No grid boxes show significance in more than 3 of the 100-yr sections. Little significance is seen anywhere following MAM ENSO events (Fig. 6a).

Considering now the 50-yr sections (10 in total), Fig. 7d for DJF is similar to Fig. 6d, with significance in the Himalayas, China, and the southern-central United States. Few grid boxes show significance in more than eight 50-yr sections. Figure 7c for SON is similar, although more significance is seen on the west coast of North America. Following JJA ENSO events, Fig. 7b, significance is very limited over North America, but still present in the Himalayas, and farther east into China. Following MAM ENSO events Fig. 7a, significance is only seen in scattered grid boxes (which could represent the 5 grid boxes out of every 100 that are expected to pass the test by chance), and rarely for more than three 50-yr sections out of a possible 10.

In conclusion, for HadCM3, the only area of the Northern Hemisphere showing a significant relationship between ENSO and SWE anomalies over any 50-yr period is the Himalayas. However, over the longer 545-yr period significant links are also present between ENSO and SWE in western and southern North America.

c. ERA-40

For ERA-40 only 38 yr of data are available after removing the 1989–94 period of poor SWE values. Figures 8 and 9 show the SWE anomaly distributions in ERA-40 following positive and negative ENSO phases,

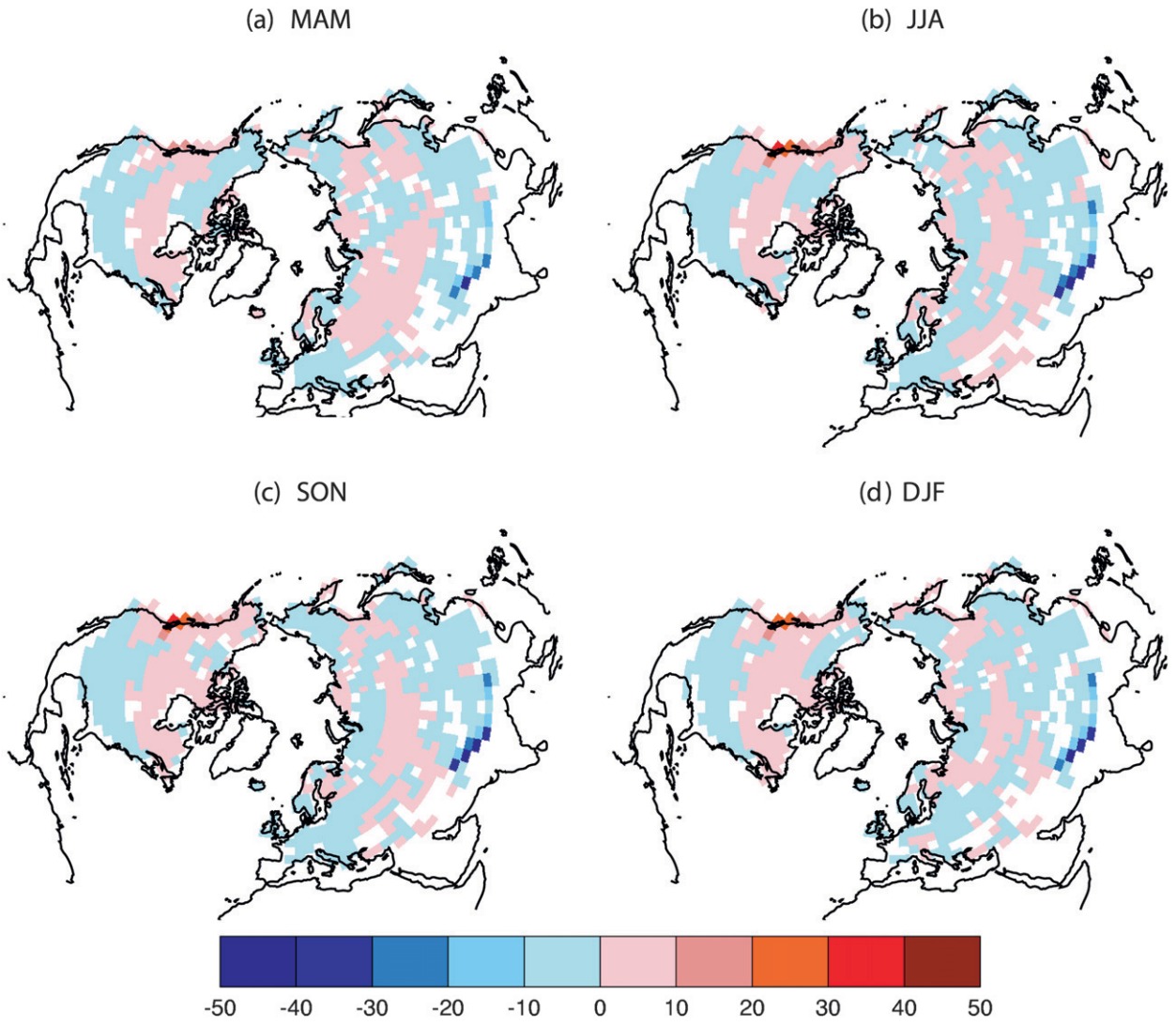

FIG. 4. As in Fig. 3, but for years with a negative ENSO index.

respectively. While the strong response seen in the GCM results in the Himalayan region is absent in these reanalysis plots, there are some broader features that are common between the two. Comparing Figs. 8 and 9 with Figs. 3 and 4, positive (negative) ENSO leads to a band of low (high) SWE values at midlatitudes, with high (low) SWE to the north and south. The pattern is clearer across North America than Eurasia. The higher-resolution ERA-40 fields show many more localized features than the low-resolution GCM fields; the patterns across North America are generally more coherent in ERA-40 than those across Eurasia, which could reflect the greater volume of assimilated SWE data in the former. An exception is the large positive anomaly seen toward the west of the continent following negative ENSO (Fig. 9).

Figure 10 shows the results of the K–S test on ERA-40 SWE anomaly composites. Overall, significance is much more scattered than for HadCM3, and significance is shifted to higher-latitude areas in both continents. February SWE anomalies coincident with DJF ENSO events show some significant response in central Asia (Fig. 10d), but there is little significance elsewhere in Eurasia or in North America. For the February SWE following SON events (Fig. 10c), significance is still present in central Asia along with the eastern Himalayas, far eastern Siberia, and a large area around the Baltic Sea. The Hudson Bay area also shows some significant grid boxes, and along the western part of the U.S.–Canada border. Scattered significant grid boxes are seen in Februaries following JJA and MAM ENSO events (Figs. 10b,a, respectively), and mainly at high latitudes.

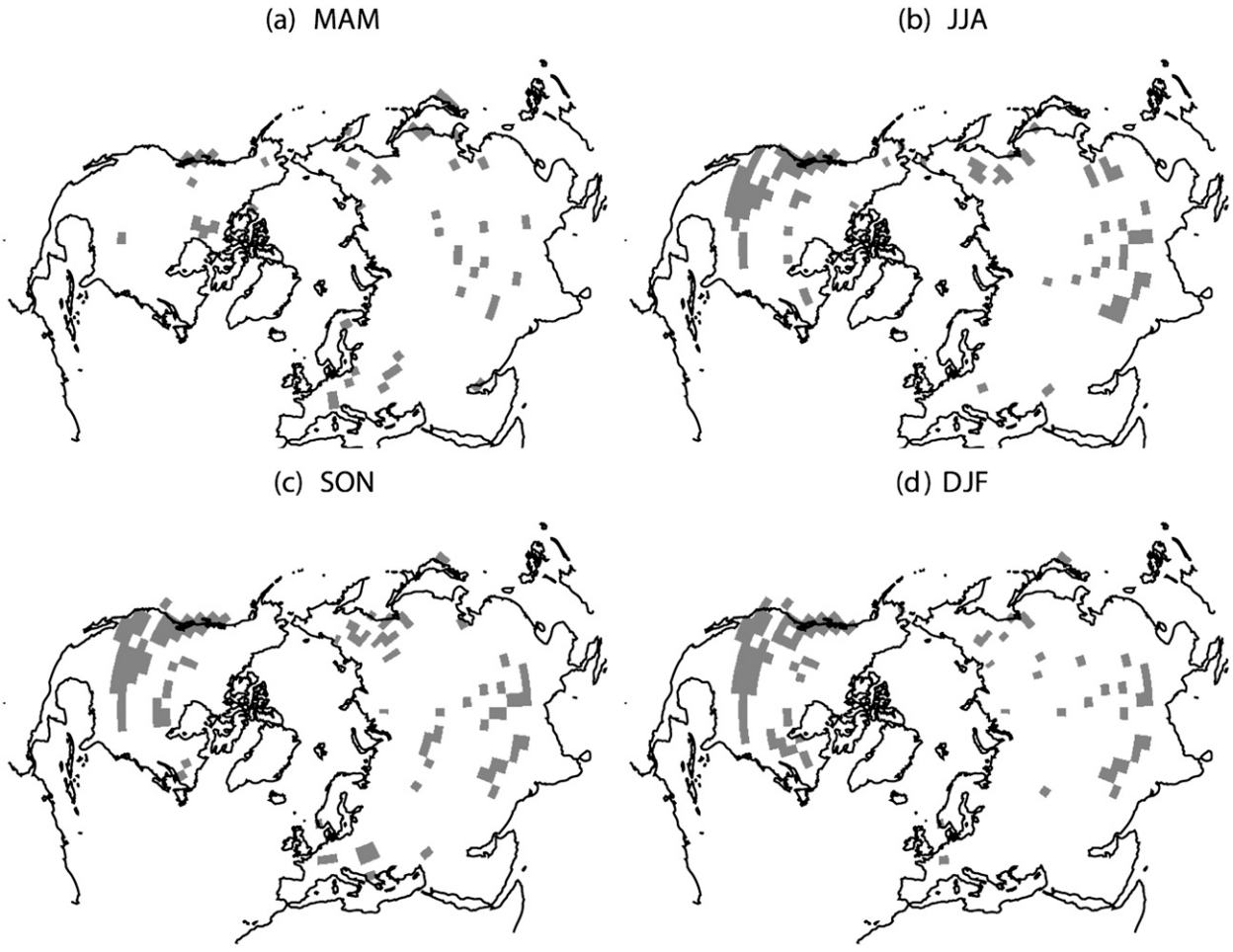

FIG. 5. HadCM3 grid boxes with significantly different frequency distribution of SWE during positive and negative ENSO phases in the 545-yr control run (threshold = 95%). Significance assessed using the K–S test.

Not all the areas that show large anomalies in the anomaly composites (Figs. 8 and 9) show significance in the K–S plots (Fig. 10). This could well occur because the K–S test is applied to the (positive event–negative event) anomalies; if positive and negative ENSO events have an impact in different grid boxes, as is more likely for the high-resolution ERA-40 data compared to HadCM3, then an individual grid box may not pass the K–S test for significance.

5. Discussion

Understanding more about the effect of well-known climate modes such as ENSO on other parts of the climate system is an important step in delivering longer-term forecasts.

This study has presented a simple experiment demonstrating the impact of ENSO phase on SWE distributions in runs of the general circulation model HadCM3, with additional comparisons made to ERA-40 reanalysis data.

The 545-yr control run shows an impact on SWE due to ENSO, which can be broadly divided into continental-scale and more local–regional-scale responses. In North America the effect of a positive ENSO event is to reduce the mean SWE and skew the distribution slightly toward lower values, and to shift the mean higher and skew the distribution toward higher values when ENSO is negative. This is associated with a continental-scale dipole anomaly structure, with anomalies of opposite sign centered in western Canada and the central United States. This dipole structure reduces the net effect of ENSO on continental mean values. This continental-scale pattern is still detectable in the 50-yr subsections, although the strongest response at longer lead times is localized over the mountainous west coast.

Some significant correlations between the ENSO phase and SWE anomalies in the Great Lakes region, as found by Sobolowski and Frei (2007), are seen in the long HadCM3 run (Figs. 5c,d), although the mean anomaly is

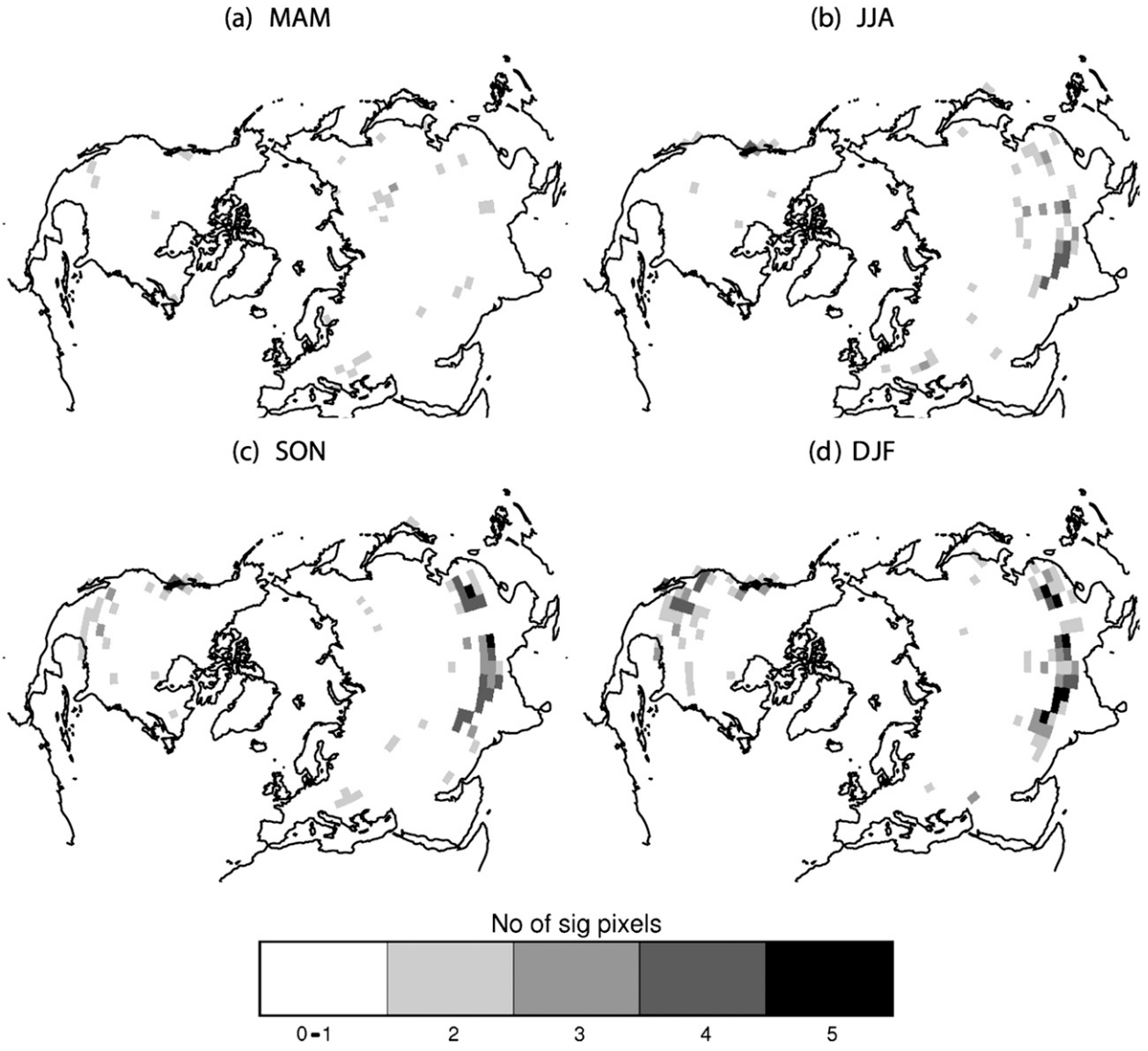

FIG. 6. HadCM3 grid boxes with significantly different SWE during positive and negative ENSO phases in the previous (a) MAM, (b) JJA, (c) SON, and (d) coincident DJF in consecutive 100-yr sections of the control run. Shading shows the number of 100-yr sections that frequency distributions at that grid box passed the K–S test (threshold = 95%).

low, and the link is not evident in the shorter subsections. Figure 10 has some shaded grid boxes showing significance in this region in the ERA-40 data. The stronger North American responses in HadCM3 are negative correlations between ENSO and SWE in western Canada, and positive correlations in the southern United States; however, weak positive correlations are seen in both these areas in the analysis of Sobolowski and Frei (2007).

In Eurasia the effect of ENSO on the frequency distribution of SWE is somewhat reversed: while warm episodes still lead to a more positively skewed distribution, the mean value is raised. Again, the opposite effect is seen during cold episodes. In Eurasia the largest anomalies are found as a localized response in the Himalayas, and it is this area that dominates the effect on continental mean SWE values, shown in Table 1. The areas showing response during both positive and negative ENSO events correspond to the regions with significantly different SWE distributions found using the K–S test. These connections are robust in the 100- and 50-yr subsections.

The positive correlation between Himalayan snow in HadCM3 and ENSO was not seen in ERA-40. However, a recent study by Mariotti (2007) of a combination of station data and reanalysis products finds a similar

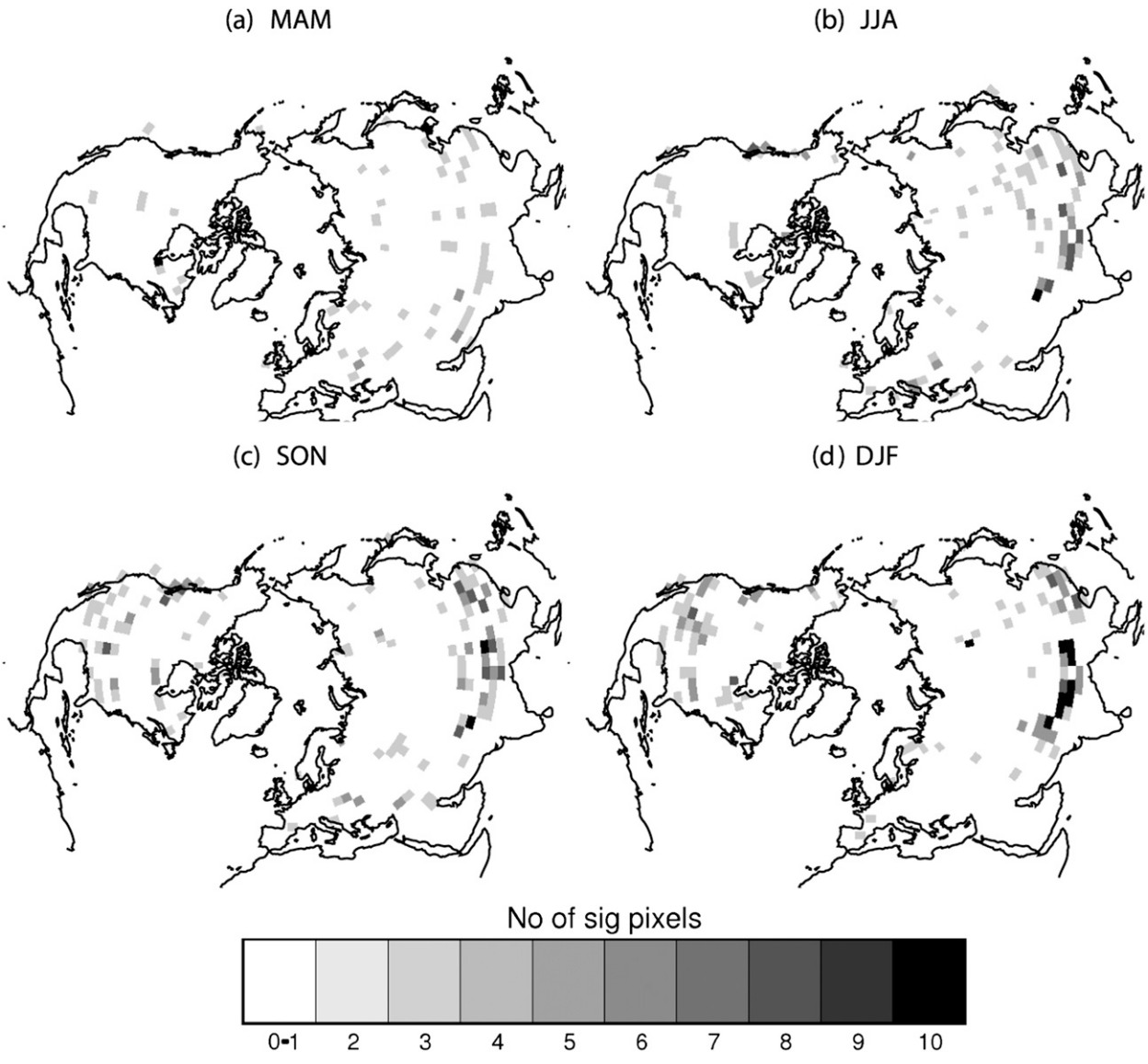

FIG. 7. As in Fig. 6, but for consecutive 50-yr sections.

relationship between SON precipitation and ENSO in this region, driven by anomalous moisture fluxes from the Arabian Sea and tropical Africa. The strong connection in the control run between ENSO and SWE in the Himalayas is worth noting in the context of snow–Indian monsoon teleconnections that have been proposed over many decades (e.g., Blanford 1884; Hahn and Shukla 1976; Robock et al. 2003). Relationships between the Asian monsoon and ENSO variability were investigated by Lau and Nath (2000). Their analysis of GCM runs, driven by observed SSTs, show positive ENSO–winter precipitation correlations much farther east than seen in the SWE distribution in HadCM3 (Figs. 3 and 4). They compare this model output with a composite of three warm events from an observation-based precipitation product that shows anomalously wet conditions over Indochina in winter, although they detect no signals in snow depth data. If the ENSO–Asian SWE connection remains undetectable in observational datasets, care must be taken in interpreting results derived from GCMs that extend these connections to monsoon prediction.

The links with February SWE distribution in the long model run are seen to exist from the previous JJA ENSO index onward. This suggests that if there is a positive or negative ENSO event occurring in JJA, characteristics of the following February SWE distribution in certain regions could be forecast, for HadCM3 at least. This

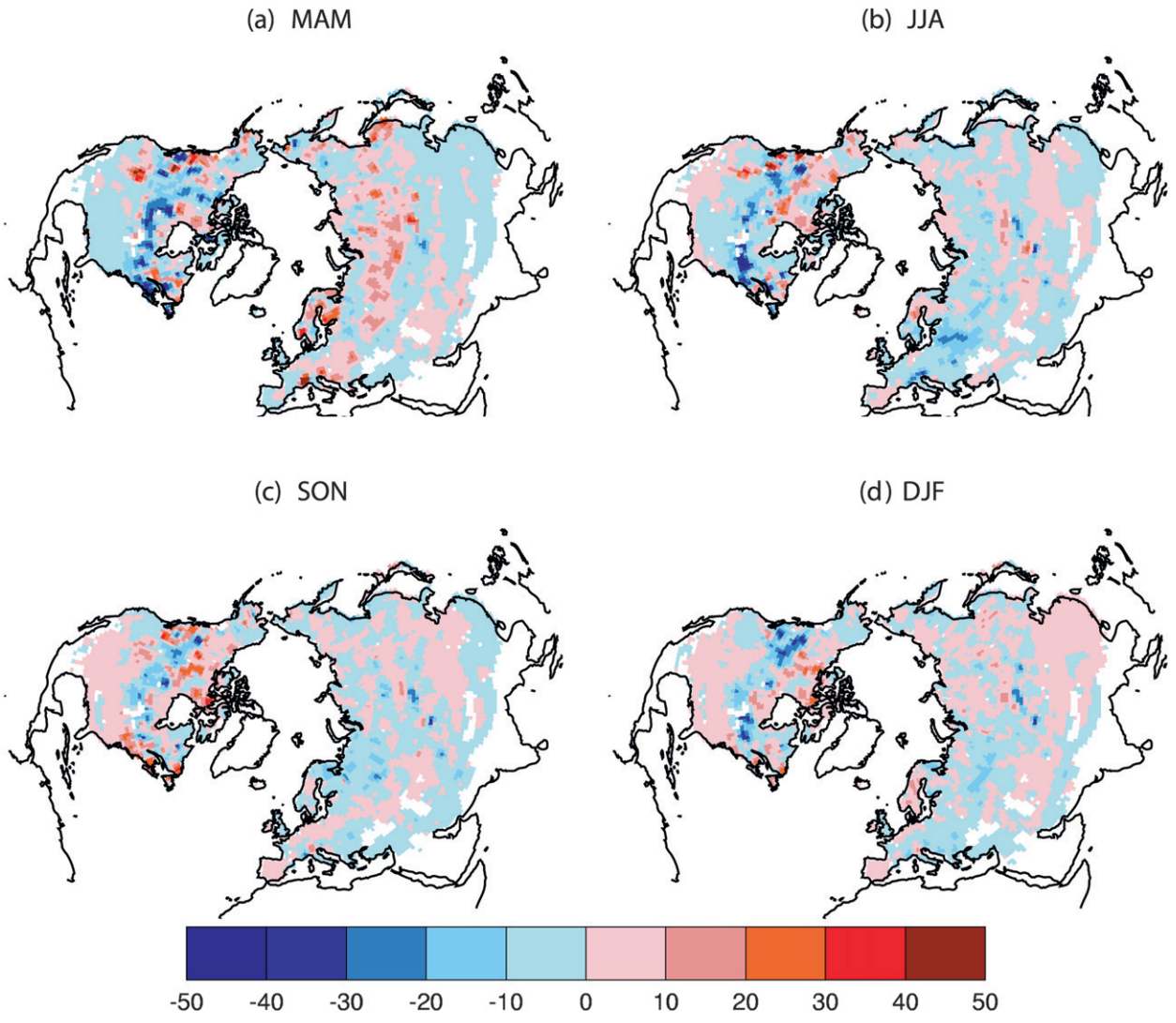

FIG. 8. February SWE anomaly distribution (mm) in ERA-40 from years with positive ENSO index in the previous (a) MAM, (b) JJA, (c) SON, and (d) coincident DJF.

would represent a long lead time to the spring runoff period (from SWE melting) for hydrological applications such as flood and wildfire forecasting. It also makes sense in terms of an ENSO event lasting several seasons, and impacting on precipitation throughout the Northern Hemisphere snow accumulation period. However, the utility of this link depends on whether the amount of variance in SWE explained by ENSO phase is high enough to be detectable in shorter time periods.

The short subsections of the HadCM3 runs show some of the features seen in the long run, but the links are weaker and the lead times much shorter. When the same approach is applied to the 38 yr of the ERA-40 reanalysis product, the pattern is somewhat changed again. The broad patterns of low SWE at midlatitudes with higher SWE bands to the north and south were reproduced for positive ENSO events, and vice versa for negative ENSO events. More scattered significance was seen across both continents in ERA-40, due to the higher-resolution (potentially more noisy) data of ERA-40, and gridbox-to-gridbox method for significance testing. Stronger correlations were seen between MAM ENSO index and February SWE than in the HadCM3 control run. This limitation on seasonal prediction within model studies has been noted before for ENSO forecasting, with the lowest predictability occurring in spring (MAM; e.g., Latif et al. 1998). This ''spring predictability barrier'' is not well understood, and it has been suggested that it is an artifact of model simulations.

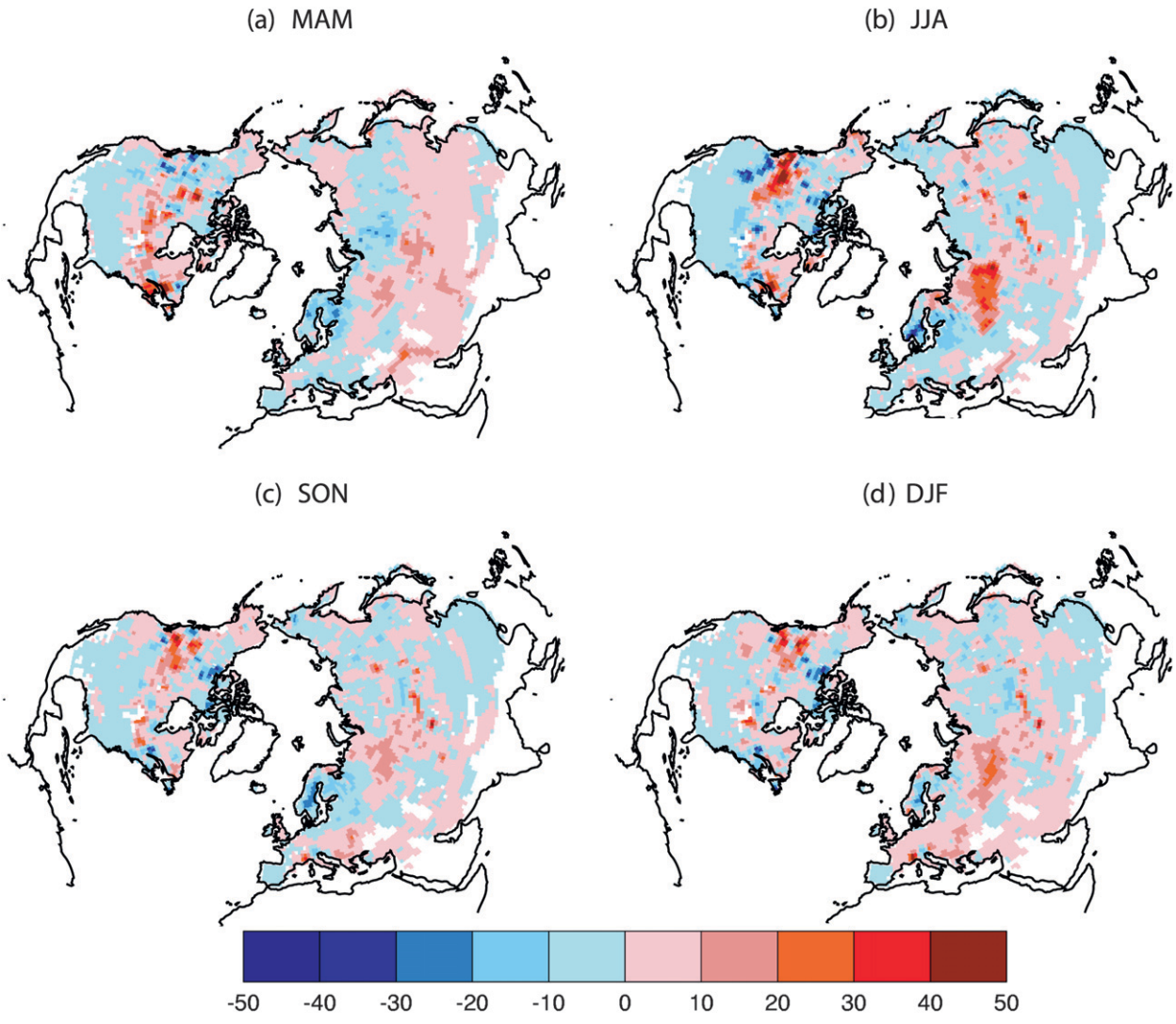

FIG. 9. As in Fig. 8, but for years with a negative ENSO index.

The most robust responses seen in North America and Eurasia are associated with mountainous regions: the west coast and Himalayas, respectively. With a gridbox size of a few hundred kilometers, the GCM is unlikely to represent precipitation patterns faithfully in these regions. Jin et al. (2006) showed that the changes in observed SWE distribution with ENSO across the western United States were driven by precipitation rather than temperature. The significant positive anomalies seen in this study in the western United States following negative ENSO events are consistent with the patterns seen in Jin et al. (2006); however, their results for warm events indicate larger positive anomalies to the south, and smaller anomalies in the mountainous regions, than are seen here. Precipitation is less well constrained than temperature in GCMs, which could explain this discrepancy.

6. Conclusions

The simple method used here has determined connections in the HadCM3 GCM between the ENSO phase and SWE in both North America and the Himalayas. While a multicentury run showed strong connections at lead times of several seasons, only local-scale connections remained over shorter time scales, and few were reproduced in the reanalysis data. Confidence in these links in the real world is limited because the signal at shorter time periods is weak, and there is a lack of suitable large-scale observational data with which to validate the results, which are predominantly in mountainous areas where GCMs are often unreliable. Using land surface fields as predictors of atmospheric variability, or vice versa as suggested here, requires confidence in both the model's representation of

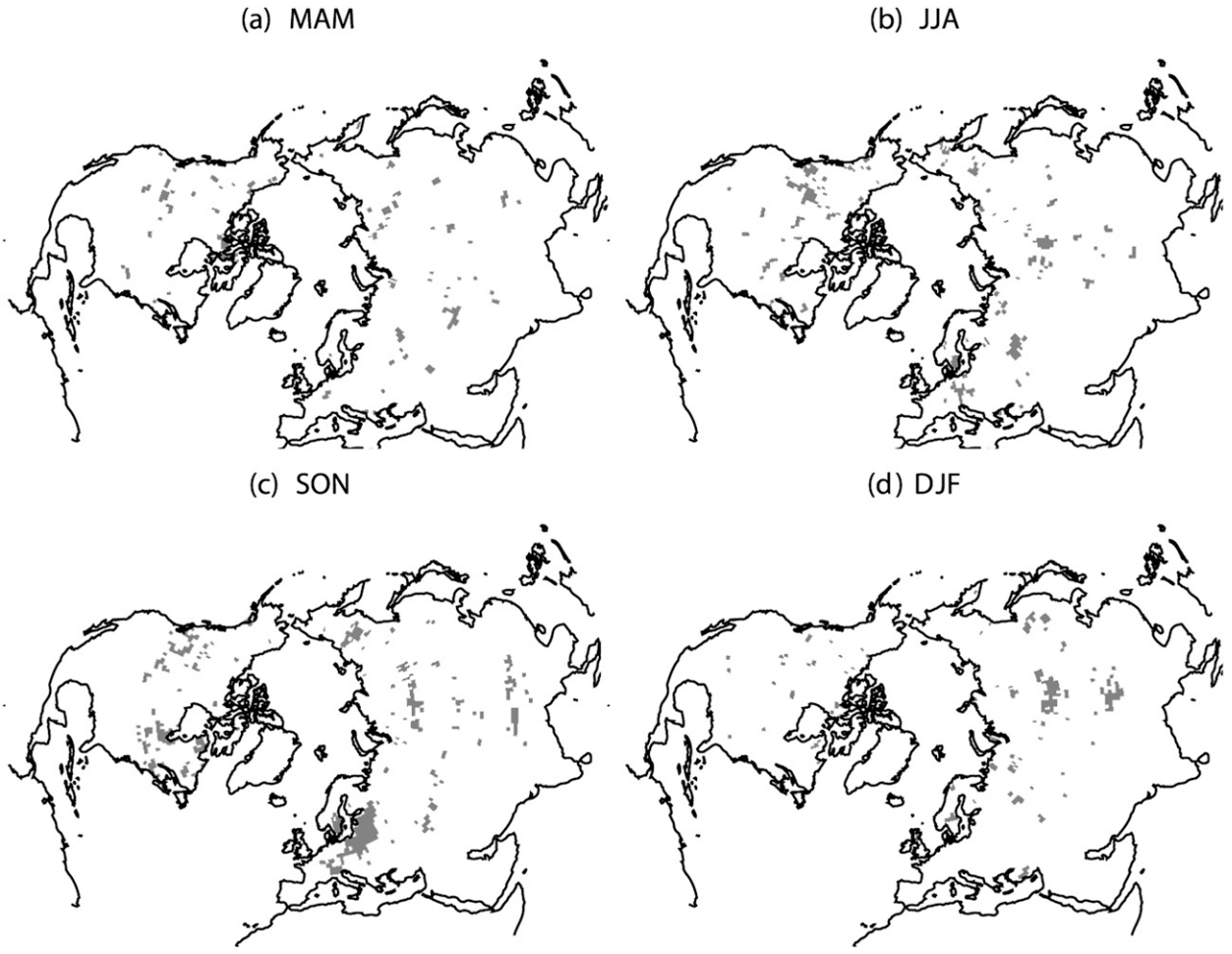

FIG. 10. ERA-40 grid boxes with significantly different frequency distribution of SWE during positive and negative ENSO phases (threshold = 95%). Significance assessed using the K–S test.

climate dynamics and its land surface component. The lack of consistency between results from observation-, reanalysis-, and model-based studies, as described above, highlights the challenge of representing real-world variability and teleconnection patterns in a GCM.

Acknowledgments. This work was funded by NERC e-Science Grant GCEP NE/C515820/1. Thanks are also due to Kevin Hodges for providing the ERA-40 data. We are grateful to Anthony Del Genio and two anonymous reviewers whose comments led to a much improved manuscript.

REFERENCES

Andreadis, K., and D. Lettenmaier, 2006: Assimilating remotely sensed snow observations into a macroscale hydrology model. *Adv. Water Resour.,* **29,** 872–886.

Armstrong, R., M. Brodzik, J. Wang, M. Savoie, O. Frauenfeld, and T. Zhang, 2004: Solutions to the snow cover mapping anomaly over the Tibetan plateau (poster). *Eos, Trans. Amer. Geophys. Union,* **85** (Fall Meeting Suppl.), Abstract C31A-0282.

Blanford, H., 1884: On the connection of the Himalaya snowfall with dry winds and seasons of drought in India. *Proc. Roy. Soc. London,* **37,** 3–22.

Brasnett, B., 1999: A global analysis of snow depth for numerical weather prediction. *J. Appl. Meteor.,* **38,** 726–740.

Brown, R., and A. Frei, 2007: Comment on ''Evaluation of surface albedo and snow cover in AR4 coupled models'' by A. Roesch *J. Geophys. Res.,* **112,** D22102, doi:10.1029/2006JD008.

——, and P. Mote, 2009: The response of Northern Hemisphere snow cover to a changing climate. *J. Climate,* **22,** 2124–2145.

——, B. Brasnett, and D. Robinson, 2003: Gridded North American monthly snow depth and snow water equivalent for GCM evaluation. *Atmos.–Ocean,* **41,** 1–14.

Clark, M., M. Serreze, and G. McCabe, 2001: Historical effects of El Niño and La Niña events on the seasonal evolution of the montane snowpack in the Columbia and Colorado river basins. *Water Resour. Res.,* **37,** 741–757.

Cohen, J., and D. Entekhabi, 1999: Eurasian snow cover variability and Northern Hemisphere climate predictability. *Geophys. Res. Lett.,* **26,** 345–348.

——, M. Barlow, P. Kushner, and K. Saito, 2007: Stratosphere–troposphere coupling and links with Eurasian land surface variability. *J. Climate,* **20,** 5335–5343.

Collins, M., S. Tett, and C. Cooper, 2001: The internal climate variability of HadCM3, a version of the Hadley Centre coupled model without flux adjustments. *Climate Dyn.,* **17,** 61–81.

Covey, C., K. AchutaRao, U. Cubasch, P. Jones, S. Lambert, M. Mann, T. Phillips, and K. Taylor, 2003: An overview of results from the Coupled Model Intercomparison Project (CMIP). *Global Planet. Change,* **37,** 103–133.

Cox, P., R. Betts, C. Bunton, R. Essery, P. Rowntree, and J. Smith, 1999: The impact of new land surface physics on the GCM simulation of climate and climate sensitivity. *Climate Dyn.,* **15,** 183–203.

Crossley, J., J. Polcher, P. Cox, N. Gedney, and S. Planton, 2000: Uncertainties linked to land-surface processes in climate change simulations. *Climate Dyn.,* **16,** 949–961.

Dai, A., I. Fung, and A. Del Genio, 1997: Surface observed global land precipitation variations during 1900–88. *J. Climate,* **10,** 2943–2962.

Derksen, C., 2008: The contribution of AMSR-E 18.7 and 10.7 GHz measurements to improved boreal forest snow water equivalent retrievals. *Remote Sens. Environ.,* **112,** 2701–2710.

Foster, D., and R. Davy, 1988: Global snow depth climatology. USAF Publ. USAFETAC/TN-88/006, U.S. Air Force Environmental Technical Applications Center, Scott Air Force Base, IL, 48 pp.

Foster, J., and Coauthors, 1996: Snow cover and snow mass intercomparisons of general circulation models and remotely sensed datasets. *J. Climate,* **9,** 409–426.

Gong, G., J. Cohen, D. Entekhabi, and Y. Ge, 2007: Hemispheric-scale climate response to Northern Eurasia land surface characteristics and snow anomalies. *Global Planet. Change,* **56,** 359–370.

Gordon, C., C. Cooper, C. Senior, H. Banks, J. Gregory, T. Johns, J. Mitchell, and R. Wood, 2000: The simulation of SST, sea ice extents, and ocean heat transports in a version of the Hadley Centre coupled model without flux adjustments. *Climate Dyn.,* **16,** 147–168.

Guilyardi, E., 2006: El Niño-mean state-seasonal cycle interactions in a multi-model ensemble. *Climate Dyn.,* **26,** 329–348.

——, and Coauthors, 2004: Representing El Niño in coupled ocean–atmosphere GCMs: The dominant role of the atmospheric component. *J. Climate,* **17,** 4623–4629.

Hahn, D., and J. Shukla, 1976: An apparent relationship between Eurasian snow cover and Indian monsoon rainfall. *J. Atmos. Sci.,* **33,** 2461–2462.

Jin, J., N. Miller, S. Sorooshian, and X. Gao, 2006: Relationship between atmospheric circulation and snowpack in the western USA. *Hydrol. Processes,* **20,** 753–767.

Latif, M., and Coauthors, 1998: A review of the predictability and prediction of ENSO. *J. Geophys. Res.,* **103,** 14 375–14 393.

Lau, N., and M. Nath, 2000: Impact of ENSO on the variability of the Asian–Australian monsoons as simulated in GCM experiments. *J. Climate,* **13,** 4287–4309.

Leathers, D., and D. Robinson, 1993: The association between extremes in North American snow cover extent and U.S. temperatures. *J. Climate,* **6,** 1345–1355.

Mariotti, A., 2007: How ENSO impacts precipitation in southwest central Asia. *Geophys. Res. Lett.,* **34,** L16706, doi:10.1029/2007GL030078.

Putt, D., 2008: Northern Hemisphere snow: Measurement, modelling and predictability. Ph.D. thesis, University of Reading, 176 pp.

Robock, A., M. Mu, K. Vinnikov, and D. Robinson, 2003: Land surface conditions over Eurasia and Indian summer monsoon rainfall. *J. Geophys. Res.,* **108,** 4131, doi:10.1029/2002JD002286.

Ropelewski, C., and M. Halpert, 1987: Global and regional scale precipitation patterns associated with the El Niño/Southern Oscillation. *Mon. Wea. Rev.,* **115,** 1606–1626.

——, and M. Bell, 2008: Shifts in the statistics of daily rainfall in South America conditional on ENSO phase. *J. Climate,* **21,** 849–865.

Shaman, J., and E. Tziperman, 2005: The effect of ENSO on Tibetan Plateau snow depth: A stationary wave teleconnection mechanism and implications for the South Asian monsoons. *J. Climate,* **18,** 2067–2079.

Slingo, J., and Coauthors, 2003: How good is the Hadley Centre climate model? Research at CGAM in identifying and understanding model systematic errors: 1999–2002. Hadley Centre Tech. Note 67, 63 pp.

Smirnov, N., 1948: Table for estimating the goodness of fit of empirical distributions. *Ann. Math. Stat.,* **19,** 279–281.

Sobolowski, S., and A. Frei, 2007: Lagged relationships between North American snow mass and atmospheric teleconnection indices. *Int. J. Climatol.,* **27,** 221–231.

Trenberth, K., 1997: The definition of El Niño. *Bull. Amer. Meteor. Soc.,* **78,** 2771–2777.

Uppala, S., and Coauthors, 2005: The ERA-40 Re-Analysis. *Quart. J. Roy. Meteor. Soc.,* **131,** 2961–3012.

van den Hurk, B., P. Viterbo, A. Beljaars, and A. Betts, 2000: Offline validation of the ERA-40 surface scheme. Tech. Memo. 295, European Centre for Medium-Range Weather Forecasts, 43 pp.

Yang, Z.-L., and Coauthors, 1999: Simulation of snow mass and extent in general circulation models. *Hydrol. Processes,* **13,** 2097–2113.

Ye, H., 2001: Characteristics of winter precipitation variation over northern-central Eurasia and their connections to sea surface temperatures over the Atlantic and Pacific Oceans. *J. Climate,* **14,** 3140–3155.